Formation Mechanisms of the Pacific–North American Teleconnection with and without Its Canonical Tropical Convection Pattern

YING DAI

Department of Atmospheric and Oceanic Sciences, School of Physics, Peking University, Beijing, China

STEVEN B. FELDSTEIN

Department of Meteorology, The Pennsylvania State University, University Park, Pennsylvania

BENKUI TAN

Department of Atmospheric and Oceanic Sciences, School of Physics, Peking University, Beijing, China

SUKYOUNG LEE

Department of Meteorology, The Pennsylvania State University, University Park, Pennsylvania, and School of Earth and Environmental Sciences, Seoul National University, Seoul, South Korea

(Manuscript received 2 June 2016, in final form 30 December 2016)

ABSTRACT

The mechanisms that drive the Pacific–North American (PNA) teleconnection pattern with and without its canonical tropical convection pattern are investigated with daily ERA-Interim and NOAA OLR data (the former pattern is referred to as the convective PNA, and the latter pattern is referred to as the nonconvective PNA). Both the convective and nonconvective positive PNA are found to be preceded by wave activity fluxes associated with a Eurasian wave train. These wave activity fluxes enter the central subtropical Pacific, a location that is favorable for barotropic wave amplification, just prior to the rapid growth of the PNA. The wave activity fluxes are stronger for the positive nonconvective PNA, suggesting that barotropic amplification plays a greater role in its development. The negative convective PNA is also preceded by a Eurasian wave train, whereas the negative nonconvective PNA grows from the North Pacific contribution to a circumglobal teleconnection pattern. Driving by high-frequency eddy vorticity fluxes is largest for the negative convective PNA, indicating that a positive feedback may be playing a more dominant role in its development.

The lifetimes of convective PNA events are found to be longer than those of nonconvective PNA events, with the former (latter) persisting for about three (two) weeks. Furthermore, the frequency of the positive (negative) convective PNA is about 40% (60%) greater than that of the positive (negative) nonconvective PNA.

1. Introduction

The Pacific–North American teleconnection pattern (PNA), characterized by a Rossby wave train with four centers of action arching from the tropical Pacific across North America, is one of the leading patterns of Northern Hemisphere midlatitude atmospheric variability (Wallace and Gutzler 1981; Barnston and Livezey 1987) [see Trenberth et al. (1998) for a review]. Among the many studies, one focus has been on the mechanisms of the growth and maintenance of the PNA.

Three mechanisms have been proposed for the development of the PNA. The first mechanism involves a poleward-propagating Rossby wave train that has been excited by tropical convection (Hoskins and Karoly 1981; Simmons 1982; Sardeshmukh and Hoskins 1988; Branstator 1985a,b; Jin and Hoskins 1995). A second mechanism involves barotropic amplification of a PNA-like disturbance due its interaction with the zonally asymmetric climatological flow (Frederiksen 1983; Simmons et al. 1983; Branstator 1990, 1992; Feldstein 2002; Franzke and Feldstein 2005; Mori and Watanabe 2008; Li and Wettstein 2012). For this mechanism, the rapid growth of the PNA arises when the wave field,

Corresponding author e-mail: Benkui Tan, bktan@pku.edu.cn

DOI: 10.1175/JCLI-D-16-0411.1

which can be generated by different physical mechanisms, including tropical convection, has a spatial structure that projects spatially onto an unstable normal mode, in this case a mode that resembles the PNA (Simmons et al. 1983). This particular modal structure is well suited to extract energy from the zonally varying climatological flow. The third mechanism involves amplification through a positive feedback onto the growing teleconnection pattern by high-frequency eddy vorticity fluxes (Egger and Schilling 1983; Lau 1988; Dole and Black 1990; Schubert and Park 1991; Branstator 1992; Black and Dole 1993; Ting and Lau 1993; Higgins and Schubert 1994; Feldstein 2002; Franzke and Feldstein 2005; Orlanski 2003, 2005). For this mechanism, the positive feedback takes place after the teleconnection pattern has been excited by other mechanisms. In studies of the PNA life cycle, Mori and Watanabe (2008) and Franzke et al. (2011) found that all three of the above mechanisms play important roles in the growth of the PNA. They showed that the PNA is first excited by tropical convection, followed by further amplification due to barotropic amplification, and driving by high-frequency eddy vorticity fluxes.

Recent studies have found that the PNA is closely related to the Madden–Julian oscillation (MJO) (Madden and Julian 1971, 1972), the dominant mode of intraseasonal variability in the tropics. The MJO is characterized by the eastward propagation of anomalies in convection through the Indian Ocean and western Pacific Ocean with a period of 30–60 days. It is found that the positive phase of the PNA occurs more frequently one to two weeks after MJO-related enhanced convection over the western Pacific Ocean and suppressed convection over the Indian Ocean, whereas the negative PNA phase shows the opposite features (Knutson and Weickmann 1987; Ferranti et al. 1990; Higgins and Mo 1997; Mori and Watanabe 2008; Johnson and Feldstein 2010; Riddle et al. 2013). Several studies on PNA life cycles have found that the breaking of synoptic-scale eddies further amplifies the convectively excited PNA: the positive PNA coincides with cyclonic wave breaking over the northeastern Pacific and the negative PNA with anticyclonic wave breaking farther to the south (Martius et al. 2007; Moore et al. 2010; Franzke et al. 2011). In a study of the relationship between tropical convection and the PNA from a continuum perspective, Johnson and Feldstein (2010) found six positive PNA-like patterns, and five negative PNA-like patterns [see Table 1 of Johnson and Feldstein (2010)]. Among these PNA-like patterns, some are associated with strong tropical convection, as in the studies discussed above, and others patterns appear to be unrelated to tropical convection. Tropical convection was the only driver that was examined in Johnson and Feldstein (2010). They did not consider the role of high-frequency eddy vorticity fluxes or barotropic amplification on the continuum of PNA-like patterns. To the best of our knowledge, none of the previous studies of PNA life cycles distinguish between PNA events that are driven by tropical convection and those that are not. Hereafter, we refer to those PNA events that are associated with the PNA's canonical tropical convection pattern as convective PNA events, and those PNA events that are not associated with this tropical convection pattern as nonconvective PNA events.

In this study, we investigate separately the formation mechanisms of these two types of PNA events. For the nonconvective PNA, one may expect barotropic amplification and/or driving by high-frequency transient eddy fluxes to take on an even more prominent role than they do in the development of the convective PNA. Furthermore, Mori and Watanabe (2008) and Franzke et al. (2011) show that the development of the positive PNA is preceded by a wave train over Eurasia, whereas the development of the negative PNA is not associated with a Eurasian wave train. Since previous studies of the PNA must have combined the convective and nonconvective PNA in their analyses, at least for the positive PNA, it is possible that the Eurasian wave train plays a more prominent role during nonconvective PNA events.

Following this section, a brief description of the data and methods used in this study is given in section 2. The main results are reported in section 3, and the summary and discussion are presented in section 4.

2. Data and methods

In this study, we use the daily (0000 UTC) European Centre for Medium-Range Weather Forecasts interim reanalysis (ERA-Interim) dataset (Dee et al. 2011). We use daily data, rather than monthly or seasonal mean data, because teleconnection patterns such as the PNA have an intrinsic time scale of about two weeks (Feldstein 2000, 2002; Cash and Lee 2001; Mori and Watanabe 2008; Johnson and Feldstein 2010; Franzke et al. 2011). The data cover the years 1979–2011 for the winter months of November–March. The ERA-Interim variables examined include 250-hPa horizontal wind and 250-hPa streamfunction. As a proxy of the occurrence and intensity of convective heating, we use the daily interpolated outgoing longwave radiation (OLR) data provided by the National Oceanic and Atmospheric Administration (Liebmann and Smith 1996). Daily anomalies at each grid point are obtained by subtracting the seasonal cycle on that calendar day. The

seasonal cycle is defined by the first three Fourier harmonics of the annual average of the daily climatology.

The PNA pattern is defined as the first empirical orthogonal function (EOF) of the 250-hPa zonal wind over the North Pacific sector (0°–87.5°N, 120°E–105°W) for the winter months, as in Athanasiadis et al. (2010). Prior to performing the EOF analysis, the gridded data are weighted by the square root of cosine of latitude (North et al. 1982). The leading principal component time series is normalized and used as the PNA index. Zonal wind, rather than the more commonly used geopotential height is used, because the zonal wind has a higher teleconnectivity than geopotential height (Athanasiadis et al. 2010). The linear correlation between the PNA index defined based on daily 250-hPa zonal wind anomalies and the more common canonical definition of Wallace and Gutzler (1981) is 0.6, statistically significant at the $p < 0.01$ level. The evolution of the PNA will be examined with composite maps of 250-hPa streamfunction.

In this study, the role of the high- and low-frequency eddies in the growth and decay of the PNA will be investigated by analyzing the horizontal divergence of the **E** vector (Hoskins et al. 1983). To this end, a 101-point Lanczos filter (Duchon 1979) with a nominal frequency cutoff period of 10 days is applied to obtain the low-frequency eddies (eddies with a period longer than 10 days) and the high-frequency eddies (eddies with a period shorter than 10 days). For this particular Lanczos filter, the 10-day high-pass (low-pass) filter response function maintains a value of 1.0 for frequencies higher (lower) than the cutoff frequency, and drops rapidly from 1 to 0 very close to the cutoff frequency. As described in Duchon (1979), a large number of weights suppresses Gibbs phenomenon. Although the entire January 1979–December 2012 dataset was filtered, we only use data from the 1979/80 to 2011/12 November–March winter seasons, thus avoiding undesirable impulse effects of the Lanczos filter.

The linkage of the PNA to tropical convection is described by the lag–lead regression of OLR in the tropics against the PNA index (Fig. 1). The most distinctive OLR feature shown in Fig. 1 is the dipolar structure with an enhanced convection center over the central tropical Pacific Ocean and a suppressed convection center over the eastern tropical Indian Ocean and the Maritime Continent. The central Pacific center undergoes slow growth from day −20 to day −10, peaking between day −10 and day −5, followed by a slow decay. In contrast, the Maritime Continent center remains relatively weak before day −10, peaking between day 0 and day +5, followed by a more rapid decay. The position of the central Pacific OLR anomaly shows little movement throughout the day −20 to day +20 time period, whereas the Maritime Continent OLR anomaly shows some eastward propagation.

In view of the fact that the relation between the positive and negative PNA may not be linear, we will consider the two phases separately. For this purpose, we perform separate composite analyses for both phases using the PNA index as a measure of the amplitude of the PNA pattern. The onset day for the positive (negative) phase of a PNA event is defined as the first day on which the PNA index exceeds 1.0 (−1.0) standard deviations and subsequently stays above (below) that threshold for at least 4 consecutive days. The day of the peak PNA index is denoted as day 0. Furthermore, two events must be at least 21 days apart. Otherwise, the weaker event is discarded.

To measure quantitatively the PNA–convection relationship, we define a convection index (CI) by projecting the daily OLR anomalies onto the two-week mean (from day −13 to day 0) OLR anomaly pattern for the domain (15°N–15°S, 60°E–120°W) shown in Fig. 1. We choose a two-week average because the regressed OLR anomalies vary slowly with time lag. A normalized CI is used as a measure of the intensity of the convection pattern with positive (negative) CI indicating enhanced (reduced) convection over the central equatorial Pacific and reduced (enhanced) convection over the eastern Indian Ocean and the Maritime Continent. A PNA event is taken to be convectively driven if the value of the 5-day running mean of the standardized CI is greater (less) than 1.0 (−1.0) at least once within the 10 days before the onset day of the PNA event. A PNA event is taken to be nonconvectively driven if the absolute value of the 5-day running mean of the standardized CI is always less than 0.75 within the 10 days before the onset day of the PNA event. The choice of this threshold is to ensure that the sample size for each group is sufficiently large for composite analysis.

Statistical significance in this study is assessed with a Monte Carlo test by calculating 1000 randomly generated composites, with the number of composites being the same as the number of PNA events. To test statistical significance, the observed composite is compared to the distribution of randomly generated composites.

Since the convective PNA events are based on a smoothed CI exceeding a threshold value of 1.0 standard deviations, given the linearity of the regression in Fig. 1, it is to be expected that the anomalous OLR for the two phases of the convective PNA will take on the pattern shown in Fig. 1 but be of opposite sign. In contrast, for the nonconvective PNA events, there is no constraint on the spatial pattern of the anomalous OLR in addition to the fact that it should not be canonical. As we will see,

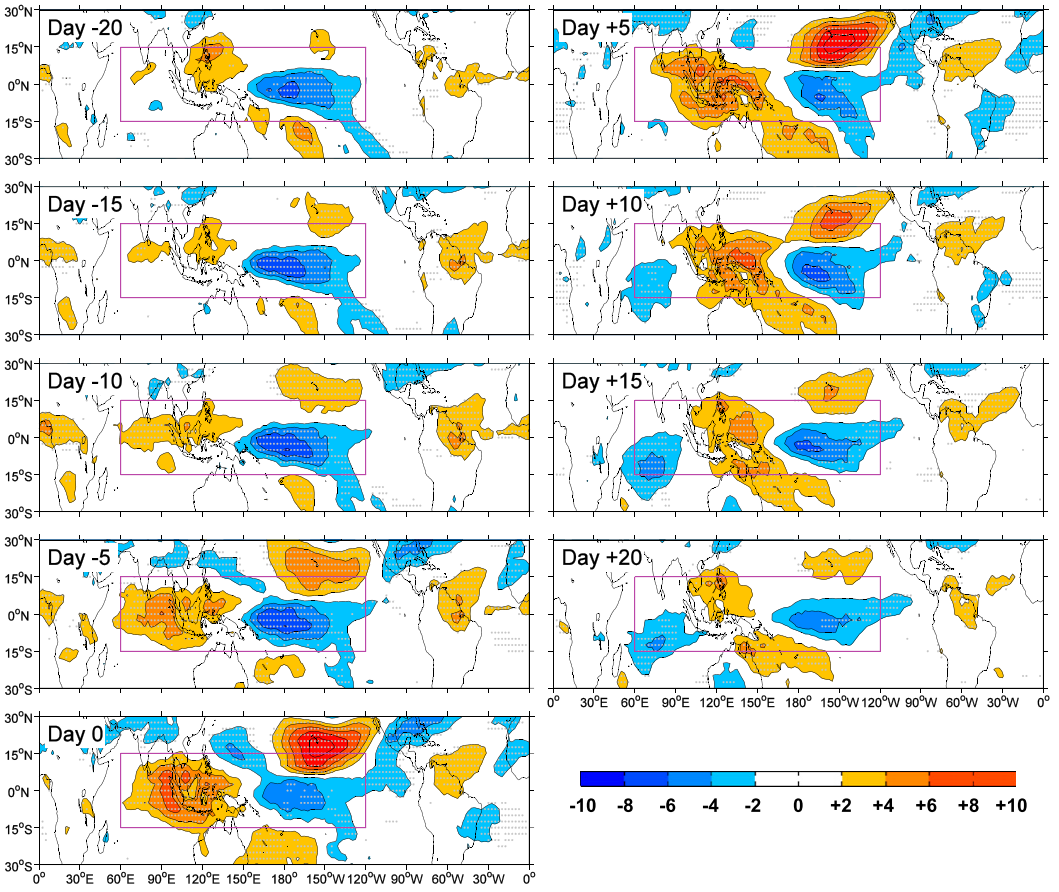

FIG. 1. Lag regressions of anomalous OLR onto the PNA index time series at lag days [−20, −15, −10, −5, 0, +5, +10, +15, +20]. The anomalies on each lag day are a pentad mean centered on that day. Warm (cold) shading denotes positive (negative) values. The contour interval is 2 W m^{-2} for OLR and zero lines are omitted. Stippling indicates OLR anomalies that are statistically significant at the $p < 0.05$ level based on the Student's t test. The purple rectangular box (15°N–15°S, 60°E–120°W) denotes the domain for calculation of the convection index.

the OLR anomalies for the positive and negative convective PNA are spatially similar, but of opposite sign, and the OLR anomalies for the positive and negative nonconvective PNA show different spatial structures from that in Fig. 1, and with a much smaller amplitude. The smaller amplitude of the nonconvective PNA events reflects the observation that a substantial fraction of the OLR variance in the tropics is associated with a dipole anomaly resembling that shown in Fig. 1. Furthermore, whenever we remark on the difference between lead–lag patterns, these comparisons are qualitative and based on the overall distribution of the pattern evolution rather than a formal statistical test.

3. Results

We have identified 47 positive phase PNA (PNA$^+$) events and 44 negative phase PNA (PNA$^-$) events in total for the period 1979–2011 (Table 1). For the PNA$^+$, there are 18 convective events (Conv$^+$; the positive convective PNA), and 13 nonconvective events (NonConv; the positive nonconvective PNA). In contrast, for the PNA$^-$, there are 18 convective events (Conv$^-$; the negative convective PNA), and 11 nonconvective events (NonConv; the negative nonconvective PNA). Note that "Conv$^+$" ("Conv$^-$") refers to PNA events with the canonical positive (negative) tropical convection pattern, and "NonConv" refers to PNA events without the canonical tropical convection pattern. This implies that PNA events, regardless of their phases, can occur with or without its canonical tropical convection pattern, and that the frequency of occurrence of the positive (negative) convective PNA is about 40% (60%) greater than that of the positive (negative) nonconvective PNA. Separating the events into early (November and December) and late (February and March) winter, it is found with the exception of November and December for the positive PNA, there are more convective than

TABLE 1. PNA events detected for the entire winter over 1979–2011. The plus sign "+" represents the positive phase, and the minus sign "−" represents the negative phase. "Conv$^+$," "Conv$^-$," and "NonConv" represent the positive-phase convection, the negative-phase convection, and PNA events without the canonical tropical convection pattern, respectively. The classification is based on five different threshold values of the CI. CI threshold values "1.0/0.75" represent +/−1.0 for the convectively driven PNA and +/−0.75 for the nonconvectively driven PNA. CI threshold values "0.9/0.85" represent +/−0.9 for the convectively driven PNA and +/−0.85 for the nonconvectively driven PNA. All the other threshold values in this table follow analogous definitions, with the first (second) value corresponding to the CI threshold for convective (nonconvective) PNA events. Events that meet none of the thresholds used to distinguish the convectively and nonconvectively driven PNA are discarded.

	Total	Threshold	Conv$^+$	Conv$^-$	NonConv
PNA$^+$	47	1.0/0.75	18	9	13
	47	0.9/0.85	20	9	16
	47	1.1/0.65	17	5	11
	47	1.2/0.55	17	4	7
	47	1.3/0.45	17	4	3
PNA$^-$	44	1.0/0.75	3	18	11
	44	0.9/0.85	3	21	14
	44	1.1/0.65	3	17	10
	44	1.2/0.55	3	14	8
	44	1.3/0.45	3	13	5

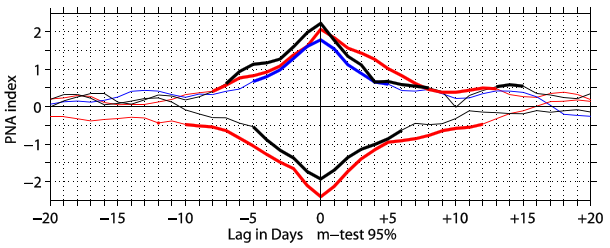

FIG. 2. Lagged composites of the normalized PNA indices. The red curves correspond to the PNA$^+$/Conv$^+$ and PNA$^-$/Conv$^-$, the black curves correspond to the PNA$^+$/NonConv and PNA$^-$/NonConv, and the blue curve corresponds to PNA$^+$/Conv$^-$. Thick lines correspond to lag days for which the composite value is statistically significant at the $p < 0.05$ level determined with a one-sided Monte Carlo test.

nonconvective PNA events. We also consider a third category of PNA event defined by the CI being of opposite sign with an amplitude and exceeding one standard deviation. For the positive PNA (Conv$^-$), there are nine events, and for the negative PNA (Conv$^+$) there are three events. In Fig. 2, we show the composite PNA indices for the five cases identified above (except for the PNA$^-$/Conv$^+$ case). As one sign for the PNA index is to be expected (e.g., when we composite the PNA index based on the positive-phase PNA events, positive values are expected), a one-sided test was used in Fig. 2. As a result, $p < 0.05$ based on a one-sided test is consistent with $p < 0.10$ based on a two-sided test.

a. Convective PNA events

We now separately examine the underlying physics of the development of the PNA for events with and without its canonical tropical convection pattern (Figs. 3 and 4). First, we examine the development of the PNA with its canonical tropical convection pattern. Composites of the anomalous 250-hPa eddy streamfunction (deviation from the zonal mean) and OLR over the 30°N–30°S band for the positive (negative) convective PNA [i.e., PNA$^+$/Conv$^+$ (PNA$^-$/Conv$^-$) events, are shown in the left column of Fig. 3 (Fig. 4)]. Composite wave activity flux vectors (Takaya and Nakamura 2001) are also calculated to illustrate snapshots of wave activity propagation. (The term "wave train" used in this study refers to a chain of positive (cyclonic) and negative (anticyclonic) streamfunction anomalies, while the wave activity fluxes indicate the direction of propagation of the wave activity that is associated with the wave trains.) From day −20 onward, the tropical OLR features for the two convective cases are similar except that they are opposite in sign. However, prior to day −14, negative OLR anomalies are observed over the North Atlantic for the negative convective PNA. Corresponding North Atlantic OLR anomalies for the positive convective PNA are not seen.

As indicated above, for the convectively driven PNA, the dipole convective anomaly is present as early as day −20 for both PNA phases. Also, at day −20 for the positive PNA (day −12 for the negative PNA), a tripole anomaly in the 250-hPa streamfunction field can be seen over the eastern Pacific (extending from south of the equator to the Gulf of Alaska), with the two northern centers serving as the North Pacific centers of the PNA. From day −10 to day 0, steady growth of the wave field (as well as the composite PNA indices in Fig. 2) is seen for both PNA phases. Beginning at day −4, based on the wave activity flux vectors, one can see that wave activity is departing from the anomalous tropical anticyclone (cyclone) for the positive (negative) PNA northeastward toward North America. These wave activity fluxes coincide with the development of the North American centers of the PNA pattern.

We see that a wave train from Eurasia may also play a role in amplifying both phases of the convective PNA. For the positive convective PNA, from day −20 to day −16, this wave train is dominated by positive anomalies over central Europe, the Arabian Sea, and Japan. By day −14, the latter two anomalies have moved westward and eastward, respectively, and a new positive anomaly developed over central Siberia. At day −12, a coherent wave train with anomalies of both signs forms

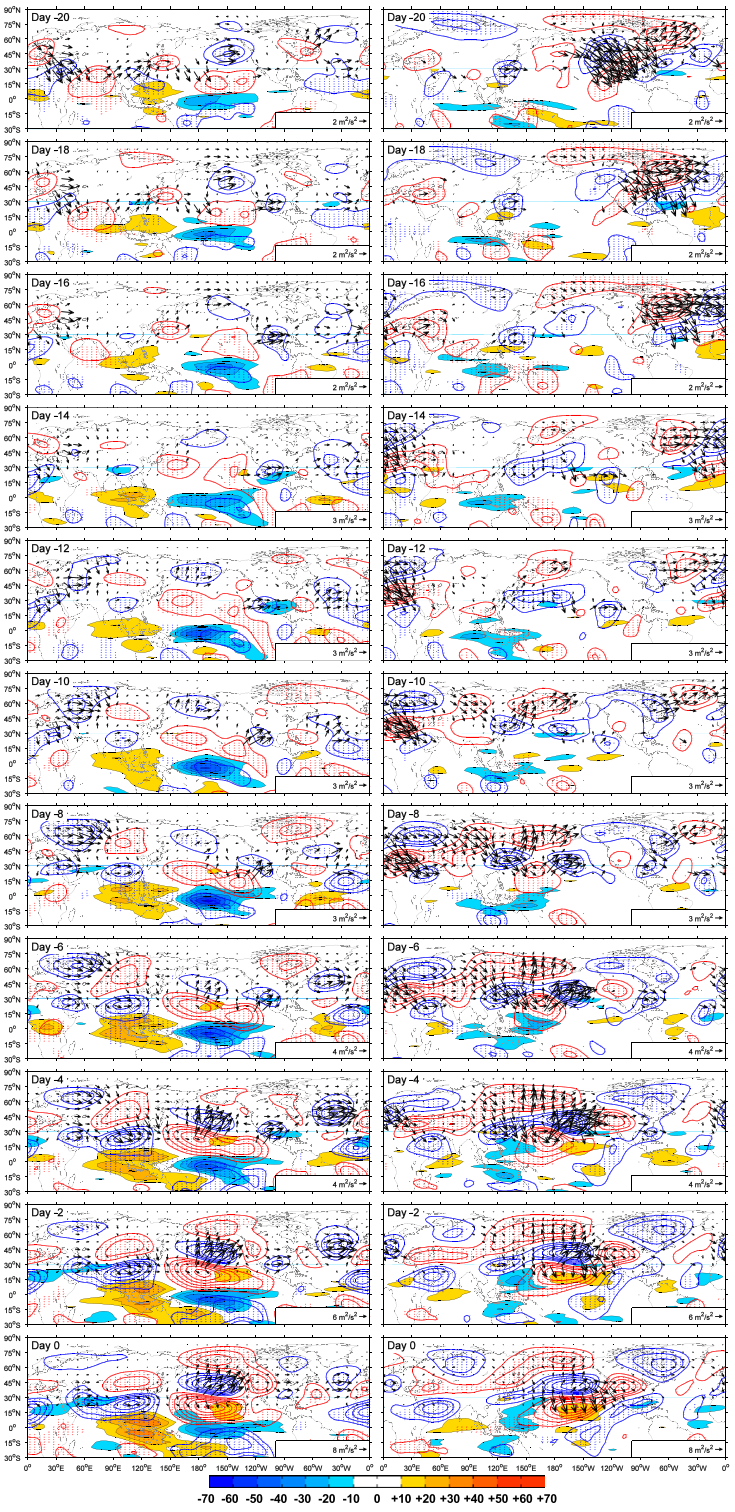

FIG. 3. Lag composites of anomalous 250-hPa eddy streamfunction (colored contours), wave activity fluxes (arrows), and OLR (shading) for the (left) PNA^+ /$Conv^+$ and (right) PNA^+/NonConv from lag day −20 to day 0 with a time interval of 2 days. Warm (cold) contours and shading indicate positive (negative) values. The contour interval is $3 \times 10^6\,m^2\,s^{-1}$ for eddy streamfunction and $10\,W\,m^{-2}$ for OLR, zero lines are omitted. Scaling for arrows is given at the bottom-right corner for each panel. Stippling indicates eddy streamfunction anomalies that are statistically significant at the $p < 0.10$ level as determined with a Monte Carlo test.

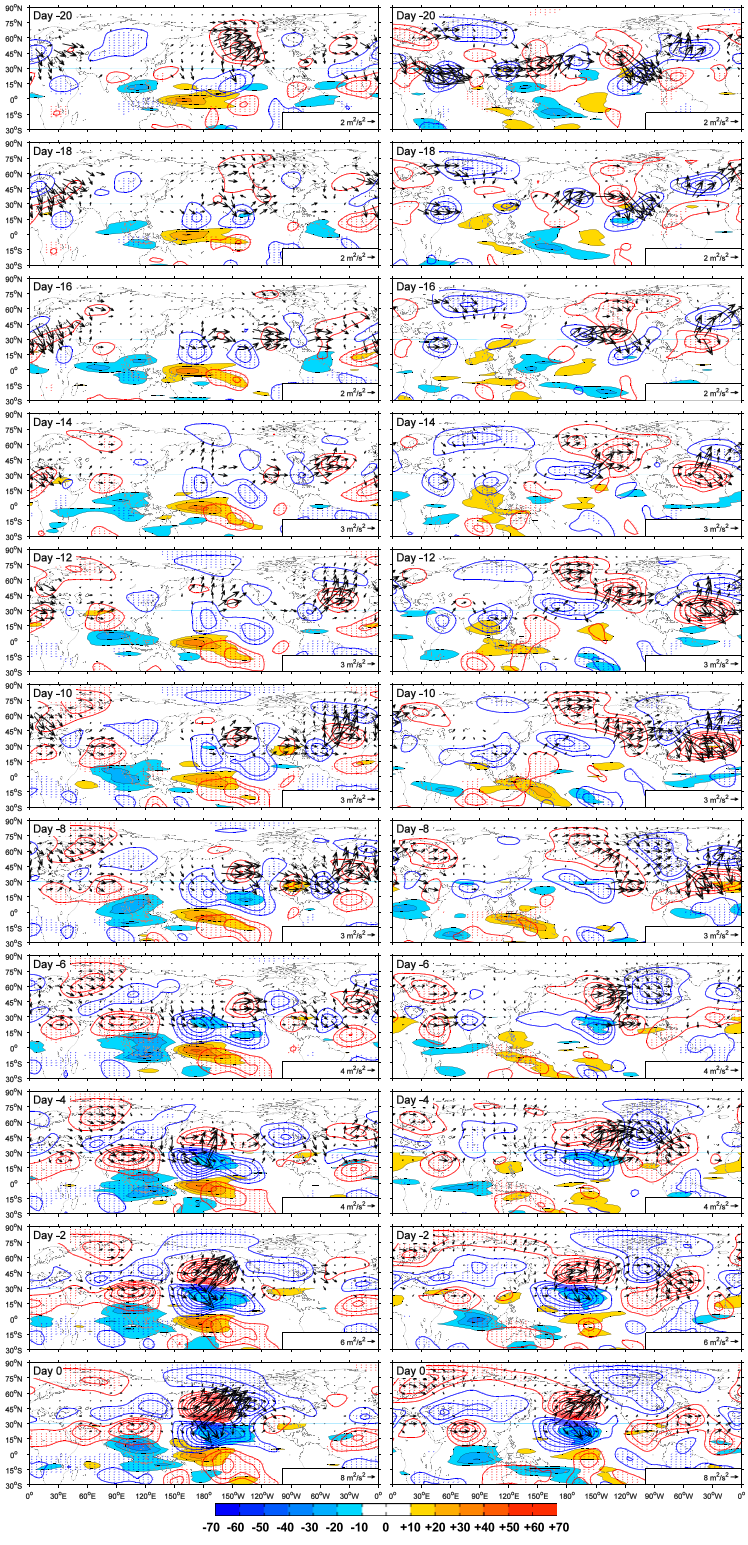

FIG. 4. As in Fig. 3, but for the (left) $PNA^-/Conv^-$ and (right) $PNA^-/NonConv$ cases.

that extends across Eurasia from northern Europe to southeastern Asia. This wave train amplifies over the following 8 days and is associated with the southeastward propagation of wave activity from Scandinavia to southeastern Asia. The wave activity fluxes reach the central subtropical Pacific at day −4. At this day, the PNA index approaches one standard deviation in amplitude (Fig. 2). The arrival of this wave train from Eurasia coincides with an increase in the growth rate of the PNA, as indicated by the larger slope of the PNA index after day −4 in Fig. 2. Likewise, for the negative convective PNA case, a similar Eurasian wave train is found to precede the growth of the PNA. Wave activity fluxes extend across Eurasia, from Europe to Southeast Asia, beginning on day −10. By day −6, these wave activity fluxes reach the central subtropical Pacific, after which the PNA undergoes more rapid growth.

The above picture suggests that the development of the positive and negative convective PNA can be viewed as a two-step process. First, anomalous dipole tropical convection precedes the PNA. Second, wave activity flux vectors associated with the Eurasian wave train reach the central subtropical Pacific, the region favored for PNA growth via barotropic amplification (Simmons et al. 1983; Feldstein 2002), at the same time that the PNA begins to undergo rapid growth. These results suggest that tropical convection first excites the PNA, and that subsequent PNA growth is due to barotropic ampification associated with the Eurasian wave train. As discussed in the introduction, Simmons et al. (1983) suggested that different mechanisms can lead to PNA growth, as long as the wave field has a spatial structure that matches an unstable normal mode. In this case, it is plausible that the wave train generated by tropical convection and the Eurasian wave train both have the appropriate structure to extract energy from the zonally asymmetric climatological flow. However, modeling calculations are necessary to provide support for this causal relationship between tropical convection, the Eurasian wave train, and the PNA. Although causality cannot be claimed based only on time–lag relationships, the above observational results are suggestive of driving of the PNA by tropical convection given the agreements in the anomalous streamfunction and tropical convection fields between the present study and those in idealized modeling papers (Matthews et al. 2004; Seo and Son 2012; Yoo et al. 2012; Goss and Feldstein 2015). (Note that when a causal relationship is stated, we are implying consistency with these modeling papers.) Furthermore, we also calculated lagged composites of the 250-hPa eddy streamfunction field (positive lags only) based on the CI. First, we defined tropical convection events with the criterion that the positive (negative) CI exceeds an amplitude of 1.0 (−1.0) standard deviations for 5 or more consecutive days, and each event must be at least 21 days apart. Then, composites of 250-hPa eddy streamfunction as a function of lag day relative to the peak day for both phases of the tropical convection events were calculated (not shown). The results reveal for positive (negative) CI events that the composite wave field at lag +6 (+4) days projects most strongly onto the PNA^+ (PNA^-) pattern. The observation that both phases of the PNA patterns are established at positive lags provides further support to our suggestion of a causal relationship between the dipole tropical convection and the PNA.

b. *Nonconvective PNA events*

Figures 3 and 4 (right columns) show lag–lead composites of the anomalous 250-hPa eddy streamfunction and OLR over the band 30°N–30°S, for the positive and negative phase PNA without its canonical tropical convection pattern (PNA^+/NonConv and PNA^-/NonConv). For the positive nonconvective PNA (Fig. 3, right column), before day −16, some weak cyclonic and anticyclonic disturbances and a large-amplitude wave train are found to occur over the North Pacific and the North America–North Atlantic sectors. These weak disturbances retrogress westward (day −20 to day −16) and gradually develop into a dipolelike anomaly over the North Pacific (day −14 to day −12). At a later time, the southern center of the dipole corresponds to the northeast Pacific center of the PNA. Over the same interval, the wave train over North America and North Atlantic disperses its wave activity eastward toward Europe, then, southward toward North Africa (from day −14 to day −12), and then eastward at day −10, which generates a wave train that extends from Europe across Siberia toward the east coast of Asia. This Eurasian wave train is observed both in the string of anomalous highs and lows across Eurasia as well as the presence of wave activity fluxes spanning the same region. This wave train, as well as the corresponding wave activity flux vectors, reach the central subtropical Pacific (the region favored for PNA growth via stationary eddy advection) by day −8, and its arrival coincides with the formation of an anomalous anticyclone in the same region. Over the time interval from day −8 to day 0, wave activity can be seen dispersing northeastward downstream from the anomalous anticyclone toward the northeast Pacific and North America, leading to the gradual development into the mature PNA pattern on day 0. Consistent with this timing, the composite PNA index is seen to begin its rapid growth at day −8 (Fig. 2).

As can be seen in Fig. 3, there are some noticeable differences in the spatial patterns of the convective and

nonconvective positive PNA between day −4 and day 0, when the PNA attains its largest amplitude. This alludes to the likelihood that the convective and nonconvective positive PNA occupy different parts of the continuum of PNA-like patterns. [Previous studies, using self-organizing map analysis, e.g., Johnson and Feldstein (2010); Lee et al. (2011); Yuan et al. (2015), have shown that the PNA is not a unique pattern, rather it can be best described as a continuum of many patterns of similar structure.] In analogy with this perspective, Johnson and Feldstein (2010) showed that the atmospheric responses to El Niño–Southern Oscillation (ENSO) and Madden–Julian oscillation (MJO) convection both project onto the canonical PNA pattern, as defined by the NOAA/Climate Prediction Center, but these responses project onto different parts of the PNA continuum. A detailed examination on this aspect of the convective and nonconvective PNA is beyond the scope of the present study.

For the negative nonconvective PNA (Fig. 4, right column), the PNA pattern appears to initiate from a circumglobal teleconnection pattern (CTP)-like wave train (zonal wavenumber 5; Branstator 2002), which is found to occur as early as lag −20 days. This CTP-like pattern includes two lows and a high over the northeast Pacific that steadily amplify and evolve into a high-over-low dipolelike anomaly over the interval from day −18 to day −12. At later times, this dipole shifts toward a lower latitude, with the southern center of the dipole reaching the central subtropical Pacific by day −6. This is followed by dispersion of wave activity northeastward toward western North America and then southeastward into the southeastern United States leading to the excitation of the two North American centers of the PNA. This downstream dispersion coincides with the amplification of the PNA from day −8 to day 0, as is seen in the composite PNA index (Fig. 2). The full PNA can be clearly observed at day 0.

The above results are consistent with the picture that the formation of the positive and negative nonconvective PNA arise from barotropic amplification. For the positive (negative) nonconvective PNA, the Eurasian (CTP-like) wave train is associated with centers entering the central subtropical Pacific, the region preferred for growth via barotropic amplification, at the same time that rapid PNA growth first takes place.

c. The $PNA^+/Conv^-$ case

We next examine the PNA formation features for the $PNA^+/Conv^-$ case (i.e., for the positive PNA phase and canonical dipole tropical convection that is of a sign opposite to that for the positive convective PNA) (Fig. 5). The anomalous dipole tropical convection can be seen at day −20 and persists through day 0. Beginning at day −20, an anomalous anticyclone at 250 hPa is present over southern Asia in a location that is consistent with driving by the enhanced convection over the eastern Indian Ocean and the Maritime Continent. Over the following 12 days, from the anomalous anticyclone, a wave train can be seen extending across the northwest Pacific toward Alaska and undergoing both amplification and eastward translation. Then, from days −10 to −6, the anomalous anticyclone over southern Asia and the anomalous cyclone east of Japan disperse southeastward and northeastward, respectively. Beginning at day −8, a wave train together with coherent wave activity fluxes that exhibit a southeastward orientation can be seen extending from Europe to central Asia. These wave activity fluxes reach the central subtropical Pacific by day −6, where the anomalous anticyclone originally over southern Asia is located. The arrival of these wave activity fluxes coincides with the rapid amplification of the anticyclone. Over the following 4 days, wave activity fluxes with a northeastward orientation are seen growing and propagating toward North America. By day −4 and day −2, the wave activity fluxes extend across Canada, and the PNA matures at day 0. This picture alludes to the possibility that enhanced convection over the eastern Indian Ocean and the Maritime Continent as well as barotropic amplification associated with the Eurasian wave train both contribute to the driving of the $PNA^+/Conv^-$. As can be seen, there are some similarities in the PNA evolution between this case and the positive nonconvective PNA, particularly in the earlier and later stages. This is an interesting point, particularly for the early stage, since the method that we use only requires that the spatial patterns resemble each other for four consecutive days in the vicinity of day 0, and the test for statistical significance is only relative to background noise. [Note that we do not examine the $PNA^-/Conv^+$ case as the sample size is too small (only three cases, see Table 1).]

d. The Eurasian wave train

For four of the five types of PNA events discussed above, strong wave activity fluxes across Eurasia were found, with the exception being the nonconvective PNA^-. We examine whether these wave activity fluxes, and the differences between these fluxes within each phase, are statistically significant. To address this question, we have composited the mean length of the horizontal (southeastward oriented) wave activity flux vectors over Eurasia for each day relative to the peak day for both phases of PNA events (Fig. 6). To examine the sensitivity of the results to the choice of the domain, two domains are chosen: one for 15°–75°N, 30°–150°E

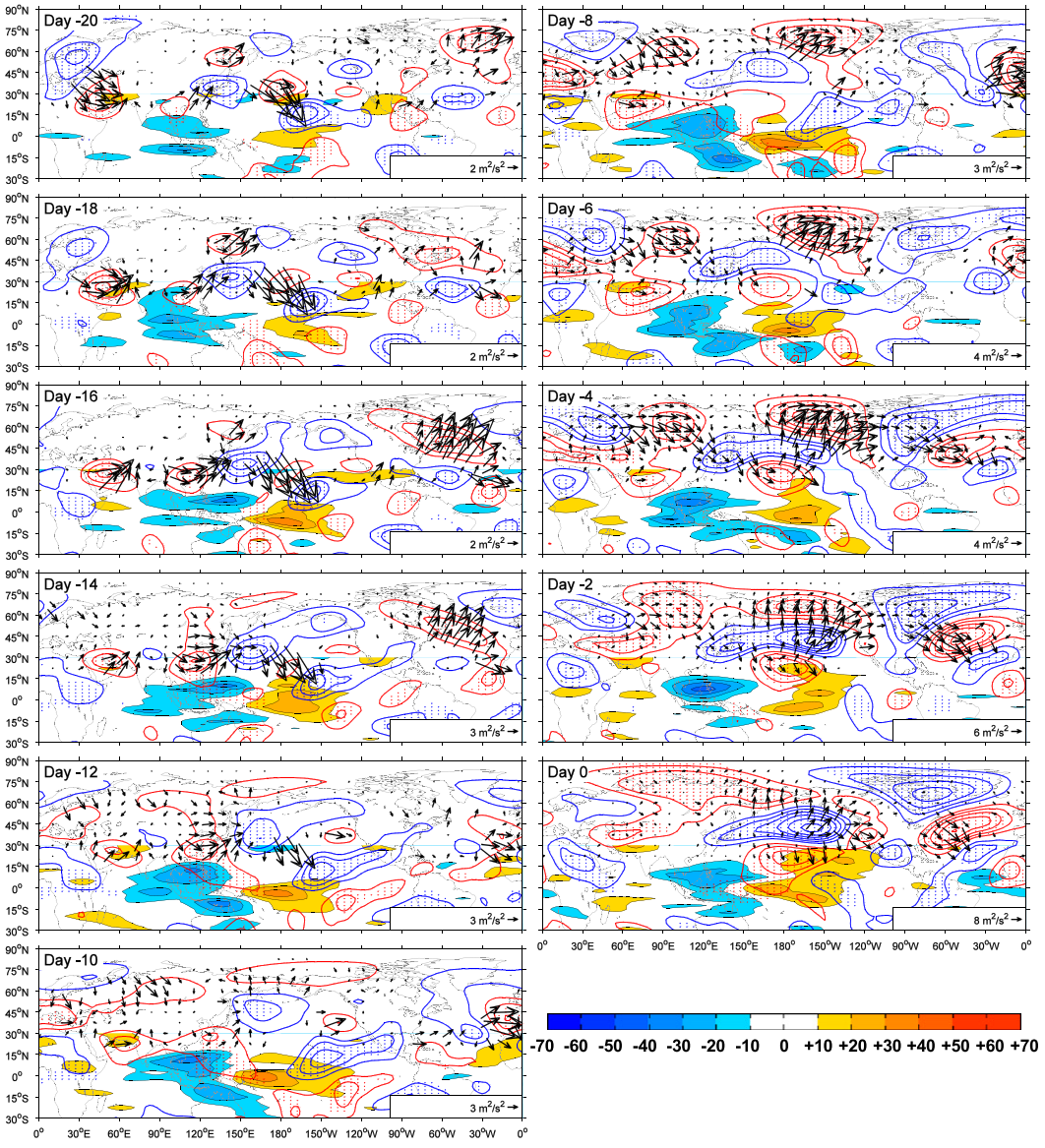

FIG. 5. As in Fig. 3, but for the $PNA^{+}/Conv^{-}$ case.

and the other for 15°–75°N, 30°E–180°. A Monte Carlo statistical significance test is performed on the mean lengths of the wave activity flux vectors. A total of 1000 random composites were performed, with the number of days specified to being the same as in the observed composites. The thick curves in Fig. 6 identify those days with wave activity flux vectors over Eurasia that have a mean length that is statistically significant at the $p < 0.10$ level. Consistent with Figs. 3–5, it can be seen from Fig. 6 that all three types of positive PNA events are preceded by large-amplitude wave activity fluxes, whereas for the negative PNA, the strong wave activity fluxes are limited to the $PNA^{-}/Conv^{-}$ events. Also, for the three positive PNA events, the $PNA^{+}/Conv^{+}$ shows the weakest wave activity fluxes. This result is also consistent with the picture, suggested above, that the nonconvective positive PNA may be driven primarily by barotropic amplification associated with the Eurasian wave train, in contrast to the positive convective PNA. Furthermore, all the PNA^{-} events, except for the $PNA^{-}/NonConv$, show statistically significant Eurasian wave activity fluxes for most of the days between day −10 and day 0.

The magenta vertical lines in Fig. 6 indicate those days for which the difference between the mean wave activity flux length for the convective and nonconvective PNA events is statistically significant at the $p < 0.10$ level. For this calculation, 1000 random difference composites are again generated. It is found that the difference in the

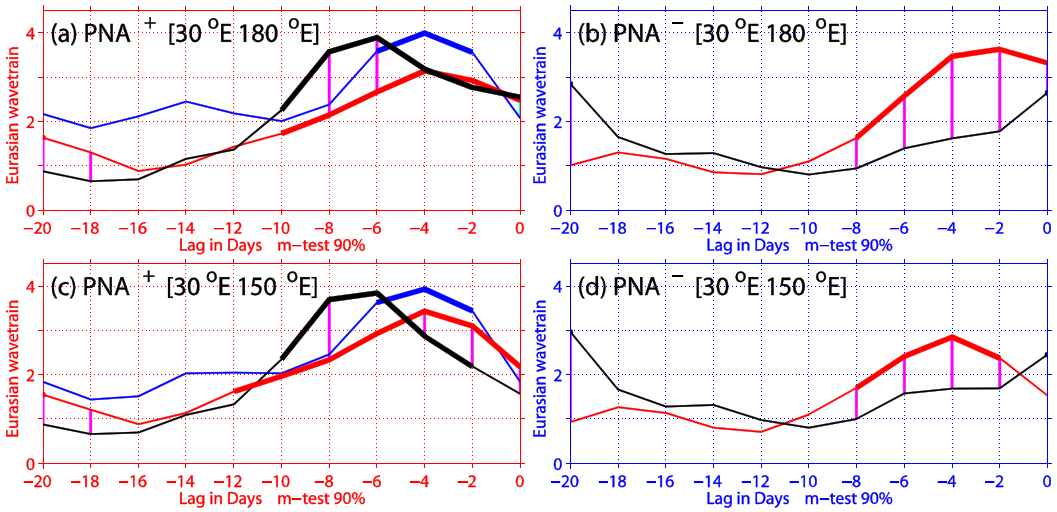

FIG. 6. Lagged composited of the mean length (units: $m^2 s^{-2}$) of the horizontal (southeastward oriented) wave activity flux vectors in the Eurasian wave train region for (a) PNA^+ and (b) PNA^- events averaged over the domain (15°–75°N, 30°E–180°); and for (c) PNA^+ and (d) PNA^- events over the domain (15°–75°N, 30°–150°E). Red curves correspond to convective PNA events, blue curves correspond to PNA events with a convection pattern that is of opposite sign to that of the convective events, and black curves correspond to nonconvective PNA events. Thick curves mark lag days for which the composite value is statistically significant at the $p < 0.10$ level determined with a Monte Carlo test. Magenta vertical lines indicate lag days for which the difference between convective and nonconvective PNA events is statistically significant at the $p < 0.10$ level as determined with a Monte Carlo test.

mean wave activity flux length between the convective and nonconvective PNA over Eurasia is statistically significant for both the PNA^+ and PNA^-. In addition, as discussed above, Fig. 6 shows the mean wave activity flux vector lengths for two Eurasian domains. As can be seen, the general relationship between the mean wave activity flux lengths for the different types of PNA events does remain the same for both domains.

e. *Time-scale features*

We next examine the time-scale characteristics of the convective and nonconvective PNA events. If we define the lifetime of a PNA event as corresponding to the time period over which its amplitude is statistically significant at the $p < 0.05$ level, then we can see that the PNA events persist for a period of about 2 to 3 weeks (Table 2). The longest lasting PNA events are those associated with the same sign of its canonical tropical convection pattern (about 3 weeks). The second longest PNA events are those without its canonical tropical convection pattern (about 2 weeks). This is the case for both the positive and negative PNA phases. The shortest PNA events are the positive PNA event with its canonical tropical convection of the opposite sign (11 days). We can gain insight into the time scale of the PNA events from the results of Branstator (2014). He showed that when anomalous tropical heating in a climate model is turned on and then off over a period of 2 days, the resulting wave train (a PNA-like wave train) persists for up to 2 weeks after the heating is turned off. This suggests that a planetary-scale Rossby wave can last for two weeks until other processes (e.g., friction, transient eddy driving, etc.) dissipate the wave train. This 2-week time scale is consistent with our findings, and suggests that a PNA wave train can persist for 2 weeks with little influence from tropical convection, but when tropical convection is strong, the PNA wave train typically lasts for one more week.

f. *Transient eddy driving*

We also examine the role of both high- and low-frequency transient eddies in the growth and decay of the PNA. For this purpose, we show composites of the zonal wind tendency (black contours) and the divergence of the **E** vector ($\overline{v'^2 - u'^2}$, $\overline{-v'u'}$) (color shadings) at 250 hPa (Fig. 7), since the local westerly (easterly) zonal wind

TABLE 2. The lifetime of PNA events with and without its canonical tropical convection pattern, defined as the time period over which the amplitude of the PNA is statistically significant at the $p < 0.05$ level determined with a one-sided Monte Carlo test.

PNA^+/$Conv^+$ 22 (days)	PNA^+/NonConv 16 (days)	PNA^+/$Conv^-$ 11 (days)
PNA^-/$Conv^-$ 23 (days)	PNA^-/NonConv 12 (days)	

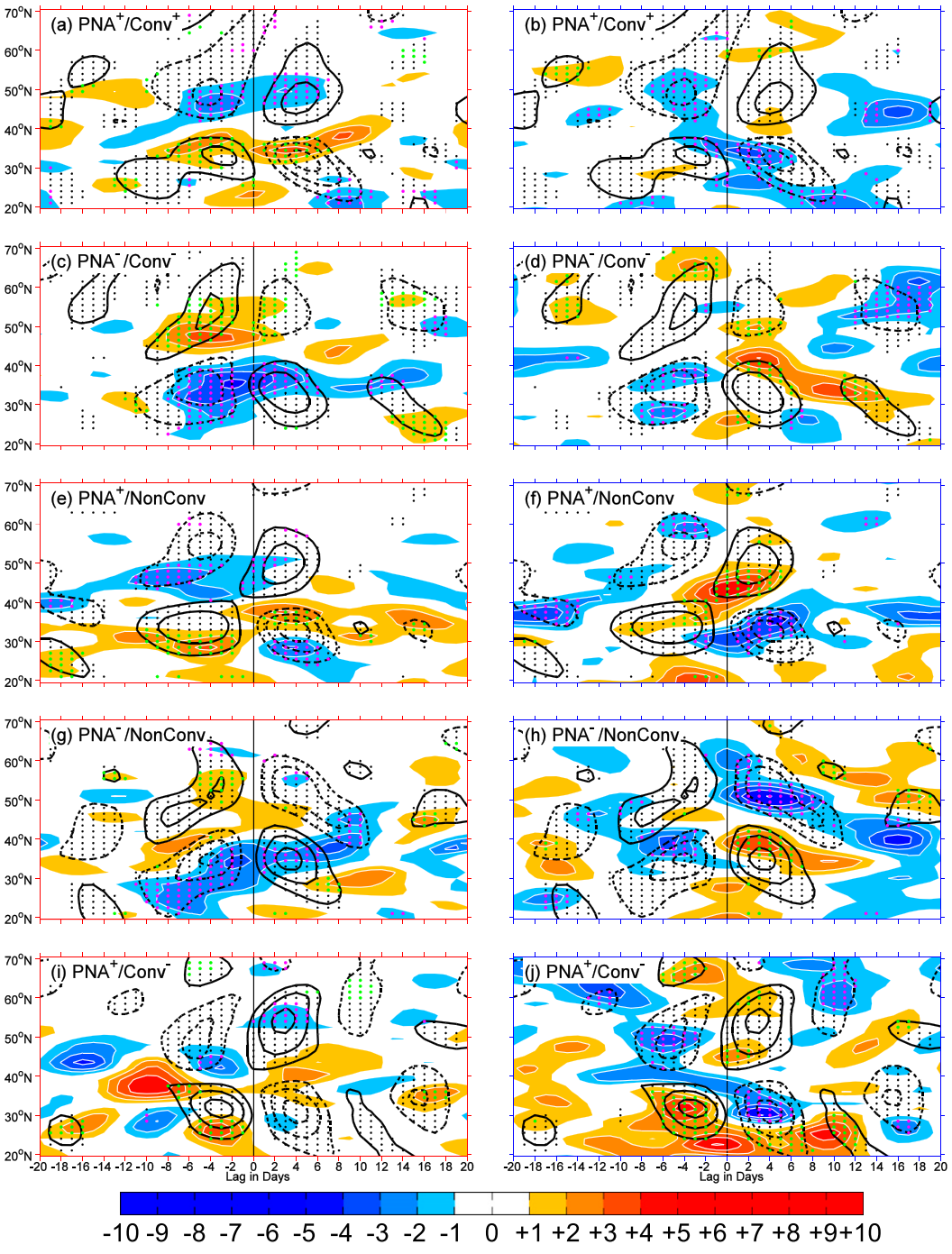

FIG. 7. (left) Composites of anomalous 250-hPa zonal wind tendency (black contours) and 10-day-high-pass-filtered **E**-vector divergence (DivE, shading) zonally averaged over the North Pacific sector (150°E–120°W) from lag −20 to +20 days for (a) $PNA^{+}/Conv^{+}$, (c) $PNA^{-}/Conv^{-}$, (e) $PNA^{+}/NonConv$, (g) $PNA^{-}/NonConv$, and (i) $PNA^{+}/Conv^{-}$. (right) As in (left), but for 10-day-low-pass-filtered DivE. Warm (cold) shading corresponds to positive (negative) values. Solid (dashed) contours indicate positive (negative) values. The contour interval is $1 \times 10^{-5}\,m\,s^{-2}$ for the zonal wind tendency and DivE. Black (color) stippling denotes anomalous zonal wind tendencies (both quantities) that are statistically significant at the $p < 0.10$ level based on a Monte Carlo test.

TABLE 3. Pattern correlation between zonal wind tendency and **E** vector divergence (DivE) over the domain from 25° to 55°N for the day −6 and day −2 time interval, and for the day 2 and day 6 time interval.

	High-pass DivE		Low-pass DivE	
	[−6 −2]	[+2 + 6]	[−6 −2]	[+2 + 6]
$PNA^+/Conv^+$	0.79	−0.72	0.48	0.70
$PNA^-/Conv^-$	0.86	−0.56	0.53	−0.16
PNA^+/NonConv	0.56	−0.10	0.19	0.79
PNA^-/NonConv	0.64	−0.39	0.51	0.81
$PNA^+/Conv^-$	0.53	−0.09	0.79	0.62

tendency is in part driven by the divergence (convergence) of the **E** vector as shown in Hoskins et al. [1983, see their Eq. (A8)]. As can be seen, for all three positive PNA cases and the two negative PNA cases, there is some meaningful overlap in the distribution of the **E** vector convergence (divergence) associated with the high-frequency eddies and the anomalous easterly (westerly) tendency before day 0, but after day 0, the zonal wind tendencies are reversed while the **E** vector divergence and convergence remain unchanged (e.g., Fig. 7, left column). This suggests that the high-frequency transient eddies contribute to the growth and the maintenance of the PNA. In contrast, in each case, there is some overlap in the distribution of the convergence (divergence) of the **E** vector associated with the low-frequency eddies and the anomalous easterly (westerly) tendency for the period from day −7 to day +7 (e.g., Fig. 7, right column), (i.e., during both the growth and the decay of the PNA). This implies that the low-frequency eddies contribute to the growth of the PNA from day −7 to day 0, but contribute to the decay of the PNA after day 0. Therefore, even though Fig. 7 shows that both high- and low-frequency transient eddies play an important role in driving each of the PNA cases, because the spatial–temporal pattern match between the **E** vector convergence and zonal wind tendencies is imperfect, the role of eddy driving of the PNA is worthy of further exploration. To evaluate quantitatively the relation between the zonal wind tendency and the **E** vector divergence, we calculate pattern correlations between the **E** vector divergence and the zonal wind tendency for the day −6 to day −2 time interval, and for the day 2 to day 6 time interval (Table 3). For all of the five groups of PNAs, for the day −6 to day −2 time interval (the growth stage), the pattern correlations between the zonal wind tendency and the high- and low-frequency **E** vector divergence are both positive, indicating that both the high- and low-frequency eddy forcing contribute to the development of PNAs. For the day 2 to day 6 time interval (the decay stage), the pattern correlations between the zonal wind tendency and the high- (low-) frequency **E** vector divergence are negative (positive, except for $PNA^-/Conv^-$), indicating that the high- (low-) frequency eddy forcing contribute to the maintenance (decay) of the PNAs.

We have also composited the difference between the high-frequency eddy forcing for the convective and nonconvective PNA events (Fig. 8). The Monte Carlo method used to test for statistical significance is the same as that for Fig. 6. It can be seen that the PNA^- different composite (Fig. 8a) for the **E** vector divergence has the form of a meridional dipole pattern centered near 40°N that is statistically significant for the day −8 to day −2 time interval, the time period when the negative PNA is growing and has an amplitude that is statistically significant (Fig. 2). This finding suggests that the negative convective PNA may be associated with a more intense high-frequency eddy feedback. This result is consistent

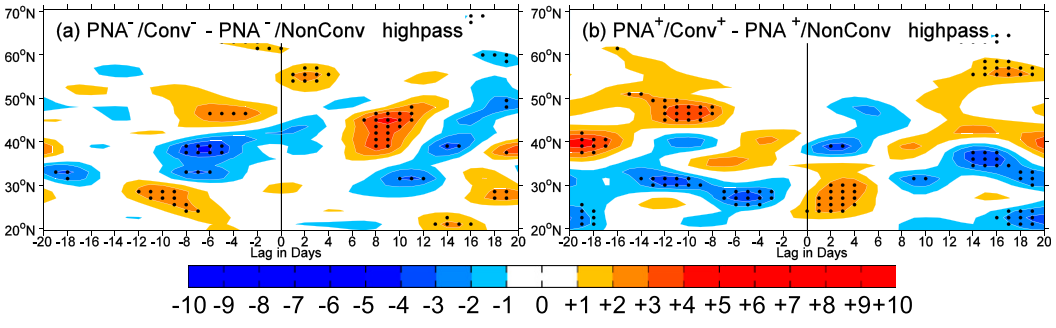

FIG. 8. The differences of composited 10-day-high-pass **E** vector divergence (shading) between (a) $PNA^-/Conv^-$ and PNA^-/NonConv (subtracting the latter from the former) and (b) $PNA^+/Conv^+$ and PNA^+/NonConv (subtracting the latter from the former). Warm (cold) shading corresponds to positive (negative) values. The contour interval is 1×10^{-5} m s^{-2}. Stippling denotes differences that are statistically significant at the $p < 0.10$ level based on a Monte Carlo test.

with that of Mori and Watanabe (2008) (when both types of PNA events are consider together) who find that the transient eddy driving is stronger for the negative PNA. For the positive PNA, there is also a statistically significant difference in the high-frequency **E** vector divergence between the convective and nonconvective events, but this occurs from day +2 to day +4 (Fig. 8b) (i.e., when the positive PNA is decaying) (Fig. 2). These results suggest that there is a statistically significant difference in the high-frequency eddy driving between convective and nonconvective PNA events for both the positive and the negative PNA.

An important question to consider is why there are differences among the various types of PNA events. An important point here is that the definition of a PNA event is that the amplitude of the PNA index must exceed one standard deviation. For the positive PNA, there is no significant difference in the high-frequency eddy driving (Fig. 8b) between the convective and nonconvective PNA^+ during PNA^+ growth (i.e., for negative lags). Furthermore, also by definition, the tropical convection is much stronger for the convective PNA^+ than for the nonconvective PNA^+. Therefore, for the nonconvective PNA^+, in order for the PNA index to exceed the threshold value, barotropic wave amplification is the only process among the three processes listed above that can account for PNA growth. Wave activity propagation across Eurasia into the jet exit region is one way that barotropic amplification can take place. For the negative PNA, both enhanced tropical convection and stronger high-frequency eddy driving (Fig. 8a) are associated with the convective PNA^-. Therefore, as for the positive PNA, in order for the PNA index to exceed the threshold value, strong barotropic wave amplification is expected to take place. In this case, for the negative nonconvective PNA, this occurs through barotropic amplification of the remnants of a circumglobal teleconnection pattern within the jet exit region.

g. *Sensitivity tests*

We tested the sensitivity of the CI-based analyses using both a much more restrictive (e.g., +/−7.5° latitude) and a much more expansive (e.g., +/−22.5° latitude) domain. The linear correlations between the CI used in this study and the other CI obtained from the more restrictive and more expansive domains were found to have a value of 0.98 in both cases. Furthermore, we also calculated composites of the anomalous 250-hPa eddy streamfunction and wave activity flux vectors for PNA events identified using the CI from these ranges of latitudes and found qualitatively consistent results with those in Figs. 3–5 (not shown). These findings suggest that the CI-based analyses are not sensitive to the range of latitudes used for projection. The sensitivity of the CI-based analyses to the particular OLR dataset is also examined by obtaining a projection pattern (analogous to Fig. 1) and CI with ERA-Interim data. A very similar OLR projection pattern was obtained (not shown), and linear correlations between the two CIs was found to have a value of 0.95, indicating that CI-based analyses are not sensitive to the particular OLR dataset.

TABLE 4. As in Table 1, but for three different thresholds of the PNA index. "Threshold" represents the critical value (unit: standard deviation) that the PNA index must exceed for four or more consecutive days to be taken as an event. When testing different thresholds for the PNA index, the CI value is kept the same. That is, the 5-day running mean CI must be greater than 1.0 at least once within the 10 days before the onset of the PNA event to identify a convectively driven PNA event, while the absolute value of the 5-day running mean CI must always be less than 0.75 for the 10 days before PNA onset to define a nonconvectively driven PNA event.

	Threshold	Total	$Conv^+$	$Conv^-$	NonConv
PNA^+	0.8	54	21	10	16
	1.0	47	18	9	13
	1.2	36	16	5	9
PNA^-	−0.8	58	3	19	22
	−1.0	44	3	18	11
	−1.2	38	2	17	9

We tested the sensitivity of the above results to the PNA index and CI threshold values. As can be seen from Tables 1 and 4, for a wide range of threshold values of the PNA and CI indices, for both the positive and negative PNA, the convective events are more frequent than the nonconvective events, which are in turn more frequent than the events with convective patterns of opposite sign. This finding shows that the relative frequencies of the various types of PNA events are not sensitive to the threshold values. In addition, we have also calculated composites of the anomalous 250-hPa eddy streamfunction and wave activity flux vectors for two cases (0.9/0.85 and 1.1/0.65) listed in Table 1 (except for those cases with threshold values of 1.3/0.45 and 1.2/0.55, since the sample size is too small for the nonconvective PNA events), and two cases (0.8 and 1.2) listed in Table 4, for the five types of PNA events (not shown). Although the spatial patterns and statistical significance are not identical to those in Figs. 3–5, the results are sufficiently similar, suggesting that our results obtained from the composite PNA evolutions are not overly sensitive to the threshold values.

4. Summary and discussion

This observational study demonstrates that the PNA patterns can be driven with or without their canonical

tropical convection pattern. The frequency of occurrence of the positive (negative) convective PNA was found to be about 40% (60%) greater than that of the positive (negative) nonconvective PNA. Furthermore, convective PNA events last longer than nonconvective PNA events, as the former persists for about 3 weeks and the latter about 2 weeks. A plausible explanation for the difference in time scale for these PNA events is simply that the convective driving during the convective PNA events lasts for about 3 weeks.

Besides the role of the tropical convection, there are important differences between the convective and nonconvective PNA events for both phases. The formation of both convective and nonconvective positive PNA events are preceded by wave activity fluxes associated with a wave train that extends across Eurasia and reaches the central subtropical Pacific (the region over the North Pacific that is favorable for stationary eddy advection) just prior to the start of rapid growth of the PNA. These wave activity fluxes are stronger for the positive nonconvective PNA. The location, timing, and amplitude of these wave activity fluxes suggest that barotropic amplification may play a larger role in amplifying the positive nonconvective PNA. For negative PNA, the development of convective and nonconvective events shows an even greater difference. The convective negative PNA is preceded by a Eurasian wave train, whereas the nonconvective negative PNA develops from amplifying northeast Pacific anomalies that are associated with a CTP-like wave train. Interestingly, the convective negative PNA exhibits stronger high-frequency eddy driving than the nonconvective negative PNA, alluding to the possibility that positive feedback plays a greater role for the convective negative PNA.

Important differences were found for the role of tropical convection, barotropic amplification, and high-frequency eddy driving during the various types of PNA events. One question that remains is how the convection and the upstream Eurasian wave train are related. Since the Eurasian wave train is stronger for nonconvective PNA events, it could be that the convective PNA is associated with a process that also weakens the Eurasian wave train. Testing this possibility requires further investigation, including idealized numerical modeling.

Acknowledgments. We thank all three anonymous reviewers for their helpful comments. This research was supported by National Natural Science Foundation of China Grants 41130962 and 41375060, National Science Foundation Grant AGS-1401220, and National Oceanic and Atmospheric Administration Grant NA14OAR4310190. The authors thank the ECMWF for making available the ERA-Interim reanalysis dataset, and NOAA/Earth System Research Laboratory/Physical Sciences Division for making available the outgoing longwave radiation data.

REFERENCES

Athanasiadis, P. J., J. M. Wallace, and J. J. Wettstein, 2010: Patterns of wintertime jet stream variability and their relation to the storm tracks. *J. Atmos. Sci.*, **67**, 1361–1381, doi:10.1175/2009JAS3270.1.

Barnston, A. G., and R. E. Livezey, 1987: Classification, seasonality and persistence of low-frequency atmospheric circulation patterns. *Mon. Wea. Rev.*, **115**, 1083–1126, doi:10.1175/1520-0493(1987)115<1083:CSAPOL>2.0.CO;2.

Black, R. X., and R. M. Dole, 1993: The dynamics of large-scale cyclogenesis over the North Pacific Ocean. *J. Atmos. Sci.*, **50**, 421–442, doi:10.1175/1520-0469(1993)050<0421:TDOLSC>2.0.CO;2.

Branstator, G., 1985a: Analysis of general circulation model sea surface temperature anomaly simulations using a linear model. Part I: Forced solutions. *J. Atmos. Sci.*, **42**, 2225–2241, doi:10.1175/1520-0469(1985)042<2225:AOGCMS>2.0.CO;2.

——, 1985b: Analysis of general circulation model sea surface temperature anomaly simulations using a linear model. Part II: Eigenanalysis. *J. Atmos. Sci.*, **42**, 2242–2254, doi:10.1175/1520-0469(1985)042<2242:AOGCMS>2.0.CO;2.

——, 1990: Low-frequency patterns induced by stationary waves. *J. Atmos. Sci.*, **47**, 629–648, doi:10.1175/1520-0469(1990)047<0629:LFPIBS>2.0.CO;2.

——, 1992: The maintenance of low-frequency atmospheric anomalies. *J. Atmos. Sci.*, **49**, 1924–1945, doi:10.1175/1520-0469(1992)049<1924:TMOLFA>2.0.CO;2.

——, 2002: Circumglobal teleconnections, the jet stream waveguide, and the North Atlantic Oscillation. *J. Climate*, **15**, 1893–1910, doi:10.1175/1520-0442(2002)015<1893:CTTJSW>2.0.CO;2.

——, 2014: Long-lived response of the midlatitude circulation and storm tracks to pulses of tropical heating. *J. Climate*, **27**, 8809–8826, doi:10.1175/JCLI-D-14-00312.1.

Cash, B. A., and S. Lee, 2001: Observed nonmodal growth of the Pacific–North American teleconnection pattern. *J. Climate*, **14**, 1017–1028, doi:10.1175/1520-0442(2001)014<1017:ONGOTP>2.0.CO;2.

Dee, D. P., and Coauthors, 2011: The ERA-Interim reanalysis: Configuration and performance of the data assimilation system. *Quart. J. Roy. Meteor. Soc.*, **137**, 553–597, doi:10.1002/qj.828.

Dole, R. M., and R. X. Black, 1990: Life cycles of persistent anomalies. Part II: The development of persistent negative height anomalies over the North Pacific Ocean. *Mon. Wea. Rev.*, **118**, 824–846, doi:10.1175/1520-0493(1990)118<0824:LCOPAP>2.0.CO;2.

Duchon, C. E., 1979: Lanczos filtering in one and two dimensions. *J. Appl. Meteor.*, **18**, 1016–1022, doi:10.1175/1520-0450(1979)018<1016:LFIOAT>2.0.CO;2.

Egger, J., and H.-D. Schilling, 1983: On the theory of the long-term variability of the atmosphere. *J. Atmos. Sci.*, **40**, 1073–1085, doi:10.1175/1520-0469(1983)040<1073:OTTOTL>2.0.CO;2.

Feldstein, S. B., 2000: The timescale, power spectra, and climate noise properties of teleconnection patterns. *J. Climate*, **13**, 4430–4440, doi:10.1175/1520-0442(2000)013<4430:TTPSAC>2.0.CO;2.

——, 2002: Fundamental mechanisms of the growth and decay of the PNA teleconnection pattern. *Quart. J. Roy. Meteor. Soc.*, **128**, 775–796, doi:10.1256/0035900021643683.

Ferranti, L., T. N. Palmer, F. Molteni, and E. Klinker, 1990: Tropical–extratropical interaction associated with the 30–60 day oscillation and its impact on medium and extended range prediction. *J. Atmos. Sci.*, **47**, 2177–2199, doi:10.1175/1520-0469(1990)047<2177:TEIAWT>2.0.CO;2.

Franzke, C., and S. B. Feldstein, 2005: The continuum and dynamics of Northern Hemisphere teleconnection patterns. *J. Atmos. Sci.*, **62**, 3250–3267, doi:10.1175/JAS3536.1.

——, ——, and S. Lee, 2011: Synoptic analysis of the Pacific–North American teleconnection pattern. *Quart. J. Roy. Meteor. Soc.*, **137**, 329–346, doi:10.1002/qj.768.

Frederiksen, J. S., 1983: A unified three-dimensional instability theory of the onset of blocking and cyclogenesis. II. Teleconnection patterns. *J. Atmos. Sci.*, **40**, 2593–2609, doi:10.1175/1520-0469(1983)040<2593:AUTDIT>2.0.CO;2.

Goss, M., and S. B. Feldstein, 2015: The impact of the initial flow on the extratropical response to Madden–Julian oscillation convective heating. *Mon. Wea. Rev.*, **143**, 1104–1121, doi:10.1175/MWR-D-14-00141.1.

Higgins, R. W., and K. C. Mo, 1997: Persistent North Pacific circulation anomalies and the tropical intraseasonal oscillation. *J. Climate*, **10**, 223–244, doi:10.1175/1520-0442(1997)010<0223:PNPCAA>2.0.CO;2.

——, and S. D. Schubert, 1994: Simulated life cycles of persistent anticyclonic anomalies over the North Pacific: Role of synoptic-scale eddies. *J. Atmos. Sci.*, **51**, 3238–3260, doi:10.1175/1520-0469(1994)051<3238:SLCOPA>2.0.CO;2.

Hoskins, B. J., and D. J. Karoly, 1981: The steady linear response of a spherical atmosphere to thermal and orographic forcing. *J. Atmos. Sci.*, **38**, 1179–1196, doi:10.1175/1520-0469(1981)038<1179:TSLROA>2.0.CO;2.

——, I. N. James, and G. H. White, 1983: The shape, propagation and mean–flow interaction of large-scale weather systems. *J. Atmos. Sci.*, **40**, 1595–1612, doi:10.1175/1520-0469(1983)040<1595:TSPAMF>2.0.CO;2.

Jin, F., and B. J. Hoskins, 1995: The direct response to tropical heating in a baroclinic atmosphere. *J. Atmos. Sci.*, **52**, 307–319, doi:10.1175/1520-0469(1995)052<0307:TDRTTH>2.0.CO;2.

Johnson, N. C., and S. B. Feldstein, 2010: The continuum of North Pacific sea level pressure patterns: Intraseasonal, interannual, and interdecadal variability. *J. Climate*, **23**, 851–867, doi:10.1175/2009JCLI3099.1.

Knutson, T. R., and K. M. Weickmann, 1987: 30–60 day atmospheric oscillations: Composite life cycles of convection and circulation anomalies. *Mon. Wea. Rev.*, **115**, 1407–1436, doi:10.1175/1520-0493(1987)115<1407:DAOCLC>2.0.CO;2.

Lau, N. C., 1988: Variability of the observed midlatitude storm tracks in relation to low-frequency changes in the circulation pattern. *J. Atmos. Sci.*, **45**, 2718–2743, doi:10.1175/1520-0469(1988)045<2718:VOTOMS>2.0.CO;2.

Lee, S., T. Gong, N. C. Johnson, S. B. Feldstein, and D. Pollard, 2011: On the possible link between tropical convection and the Northern Hemisphere Arctic surface air temperature change between 1958 and 2001. *J. Climate*, **24**, 4350–4367, doi:10.1175/2011JCLI4003.1.

Li, C., and J. Wettstein, 2012: Thermally driven and eddy-driven jet variability in reanalysis. *J. Climate*, **25**, 1587–1596, doi:10.1175/JCLI-D-11-00145.1.

Liebmann, B., and C. A. Smith, 1996: Description of a complete (interpolated) outgoing longwave radiation dataset. *Bull. Amer. Meteor. Soc.*, **77**, 1275–1277.

Madden, R. A., and P. R. Julian, 1971: Detection of a 40–50 day oscillation in the zonal wind in the tropical Pacific. *J. Atmos. Sci.*, **28**, 702–708, doi:10.1175/1520-0469(1971)028<0702:DOADOI>2.0.CO;2.

——, and ——, 1972: Description of global-scale circulation cells in the tropics with a 40–50 day period. *J. Atmos. Sci.*, **29**, 1109–1123, doi:10.1175/1520-0469(1972)029<1109:DOGSCC>2.0.CO;2.

Martius, O., C. Schwierz, and H. C. Davies, 2007: Breaking waves at the tropopause in the wintertime Northern Hemisphere: Climatological analyses of the orientation and the theoretical LC1/2 classification. *J. Atmos. Sci.*, **64**, 2576–2592, doi:10.1175/JAS3977.1.

Matthews, A. J., B. J. Hoskins, and M. Masutani, 2004: The global response to tropical heating in the Madden–Julian oscillation during the northern winter. *Quart. J. Roy. Meteor. Soc.*, **130**, 1991–2011, doi:10.1256/qj.02.123.

Moore, R. W., O. Martius, and T. Spengler, 2010: The modulation of the subtropical and extratropical atmosphere in the Pacific basin in response to the Madden–Julian oscillation. *Mon. Wea. Rev.*, **138**, 2761–2779, doi:10.1175/2010MWR3194.1.

Mori, M., and M. Watanabe, 2008: The growth and triggering mechanisms of the PNA: A MJO-PNA coherence. *J. Meteor. Soc. Japan*, **86**, 213–236, doi:10.2151/jmsj.86.213.

North, G. R., F. J. Moeng, T. L. Bell, and R. F. Cahalan, 1982: The latitude dependence of the variance of zonally averaged quantities. *Mon. Wea. Rev.*, **110**, 319–326, doi:10.1175/1520-0493(1982)110<0319:TLDOTV>2.0.CO;2.

Orlanski, I., 2003: Bifurcation in eddy life cycles: Implications for storm track variability. *J. Atmos. Sci.*, **60**, 993–1023, doi:10.1175/1520-0469(2003)60<993:BIELCI>2.0.CO;2.

——, 2005: A new look at the Pacific storm track variability: Sensitivity to tropical SSTs and to upstream seeding. *J. Atmos. Sci.*, **62**, 1367–1390, doi:10.1175/JAS3428.1.

Riddle, E. E., M. B. Stoner, N. C. Johnson, M. L. L'Heureux, D. C. Collins, and S. B. Feldstein, 2013: The impact of the MJO on clusters of wintertime circulation anomalies over the North American region. *Climate Dyn.*, **40**, 1749–1766, doi:10.1007/s00382-012-1493-y.

Sardeshmukh, P. D., and B. J. Hoskins, 1988: The generation of global rotational flow by steady idealized tropical divergence. *J. Atmos. Sci.*, **45**, 1228–1251, doi:10.1175/1520-0469(1988)045<1228:TGOGRF>2.0.CO;2.

Schubert, S. D., and C.-K. Park, 1991: Low-frequency intraseasonal tropical–extratropical interactions. *J. Atmos. Sci.*, **48**, 629–650, doi:10.1175/1520-0469(1991)048<0629:LFITEI>2.0.CO;2.

Seo, K.-H., and S.-W. Son, 2012: The global atmospheric circulation response to tropical diabatic heating associated with the Madden–Julian oscillation during northern winter. *J. Atmos. Sci.*, **69**, 79–96, doi:10.1175/2011JAS3686.1.

Simmons, A. J., 1982: The forcing of stationary wave motion by tropical diabatic heating. *Quart. J. Roy. Meteor. Soc.*, **108**, 503–534, doi:10.1002/qj.49710845703.

——, J. M. Wallace, and G. W. Branstator, 1983: Barotropic wave propagation and instability, and atmospheric teleconnection patterns. *J. Atmos. Sci.*, **40**, 1363–1392, doi:10.1175/1520-0469(1983)040<1363:BWPAIA>2.0.CO;2.

Takaya, K., and H. Nakamura, 2001: A formulation of a phase-independent wave-activity flux for stationary and migratory quasigeostrophic eddies on a zonally varying basic flow. *J. Atmos. Sci.*, **58**, 608–627, doi:10.1175/1520-0469(2001)058<0608:AFOAPI>2.0.CO;2.

Ting, M., and N.-C. Lau, 1993: A diagnostic and modeling study of the monthly mean wintertime anomalies appearing in a 100-year GCM experiment. *J. Atmos. Sci.*, **50**, 2845–2867, doi:10.1175/1520-0469(1993)050<2845:ADAMSO>2.0.CO;2.

Trenberth, K. E., G. W. Branstator, D. Karoly, A. Kumar, N. Lau, and C. Ropelewski, 1998: Progress during TOGA in understanding and modeling global teleconnections associated with tropical sea surface temperatures. *J. Geophys. Res.*, **103**, 14 291–14 324, doi:10.1029/97JC01444.

Wallace, J. M., and D. S. Gutzler, 1981: Teleconnections in the geopotential height field during the Northern Hemisphere winter. *Mon. Wea. Rev.*, **109**, 784–812, doi:10.1175/1520-0493(1981)109<0784:TITGHF>2.0.CO;2.

Yoo, C., S. Lee, and S. B. Feldstein, 2012: Arctic response to an MJO-like tropical heating in an idealized GCM. *J. Atmos. Sci.*, **69**, 2379–2393, doi:10.1175/JAS-D-11-0261.1.

Yuan, J., B. Tan, S. B. Feldstein, and S. Lee, 2015: Wintertime North Pacific teleconnection patterns: Seasonal and interannual variability. *J. Climate*, **28**, 8247–8263, doi:10.1175/JCLI-D-14-00749.1.